Final Report

Project Title: Bioavailability of Fe(III) in Natural Soils and the Impact on Mobility of Inorganic Contaminants

Authors: David S. Kosson, Chair, Department of Civil and Environmental Engineering, Vanderbilt University, Nashville, TN

Robert M. Cowan, Department of Environmental Science, Rutgers University, New Brunswick, NJ

Lily Y. Young, Biotechnology Center for Agriculture and the Environment, Rutgers University, New Brunswick, NJ

Eric L. Hacherl, Department of Civil and Environmental Engineering, Vanderbilt University, Nashville, TN

David J. Scala, Department of Civil and Environmental Engineering, Vanderbilt University, Nashville, TN

Grant Number: DE-FG02-98ER62690

Abstract

Inorganic contaminants, such as heavy metals and radionuclides, can adhere to insoluble Fe(III) minerals resulting in decreased mobility of these contaminants through subsurface environments. Dissimilatory Fe(III)-reducing bacteria (DIRB), by reducing insoluble Fe(III) to soluble Fe(II), may enhance contaminant mobility. The Savannah River Site, South Carolina (SRS), has been subjected to both heavy metal and radionuclide contamination.

The overall objective of this project is to investigate the release of inorganic contaminants such as heavy metals and radionuclides that are bound to solid phase soil Fe complexes and to elucidate the mechanisms for mobilization of these contaminants that can be associated with microbial Fe(III) reduction. This is being accomplished by (i) using uncontaminated and contaminated soils from SRS as prototype systems, (ii) evaluating the diversity of DIRBs within the samples and isolating cultures for further study, (iii) using batch microcosms to evaluate the bioavailability of Fe(III) from pure minerals and SRS soils, (iv) developing kinetic and mass transfer models that reflect the system dynamics, and (v) carrying out soil column studies to elucidate the dynamics and interactions amongst Fe(III) reduction, remineralization and contaminant mobility.

This project was initiated by the PI, Professor Kosson, at Rutgers University. Subsequently, Professor Kosson relocated to Vanderbilt University and the project was transferred to Vanderbilt. This report is a summary of the research that was carried out at Rutgers and serves as a final report for that portion of the project. Many of the efforts initiated at Rutgers are currently continuing at Vanderbilt and several manuscripts are either in review or development. As such, they will cite both grant numbers (for Rutgers and Vanderbilt) in the acknowledgements.

DISCLAIMER

DISCLAIMER

Portions of this document may be illegible in electronic image products. Images are produced from the best available original document.

Introduction

Our overall objective is to investigate the release of inorganic contaminants such as heavy metals and radionuclides that are bound to solid phase soil Fe complexes and to elucidate the mechanisms for mobilization of these contaminants that can be associated with microbial Fe(III) reduction. In particular, we hypothesize that heavy metals and radionuclides bound to structured or amorphous Fe(III) oxides will be released during reduction of Fe(III) to soluble Fe(II) or to Fe(II)-bearing minerals (e.g. magnetite). Further, the increase in mobility of inorganic contaminants will depend on factors that affect bioavailability of soil Fe(III).

This project was initiated by the PI, Professor Kosson, at Rutgers University. Subsequently, Professor Kosson relocated to Vanderbilt University and the project was transferred to Vanderbilt. This report is a summary of the research that was carried out at Rutgers and serves as a final report for that portion of the project. Many of the efforts initiated at Rutgers are currently continuing at Vanderbilt and several manuscripts are either in review or development. As such, they will cite both grant numbers (for Rutgers and Vanderbilt) in the acknowledgements.

Approach

We have divided our approach into five steps. First, we have collected soil and sediment samples from the U.S. DOE Savannah River Site and characterized them physically, chemically and microbiologically. We feel that it is important to be able to frame our research results in terms of soils specific to such a site. Second, we have carried out batch microcosm studies to evaluate the bioavailability of Fe(III) from pure minerals and SRS soils. Third, we are developing a kinetics model describing microbial Fe(III) reduction and use simple batch experiments to determine model parameters. Fourth, we are incorporate this kinetics model into an existing multi-domain transport model and using continuous flow soil column experiments to determinate transport model parameters. The kinetics and transport models will allow us to predict the impact of microbial Fe(III) reduction to particular soils at the SRS site. Finally, we will conduct continuous flow column studies on the mobility of radionuclides in SRS soils as a function of microbial Fe(III) reduction. Combined with the modeling efforts, this will allow us to better understand the relationship between microbial Fe(III) reduction and radionuclide mobility.

Determination of Fe(III) bioavailability using batch microcosms and development of the kinetics model for batch systems was initiated under the grant to Rutgers and is continuing under the grant to Vanderbilt. Thus, only a summary of the results is presented here. Incorporation of the kinetics model into mass transfer modeling to simulate flow systems and execution of the continuous flow soil columns is being carried out under the grant to Vanderbilt and is not reported here.

Results

I. SRS Soils and Sediments

Soil/Sediment collection

Sediment samples were collected from floodplains at SRS that are subjected to alternating periods of oxidizing and reducing conditions. Lake-bottom sediment samples and floodplain soil samples were collected from Par Pond and Lower Three Runs (LTR) respectively. Enrichment cultures were set up as a 10% (vol. / vol.) sediment slurry in a minimal media or in water collected at the site. Amorphous FeOOH was added at ~50mM, and acetate at 10mM. Duplicate enrichments were started with 4 sediments from Par Pond (labeled P1-P4) and 3 soils from LTR. (D1, S1, T1). The cultures were incubated at room temperature in the dark without shaking. Strict anaerobic procedures were followed at all times. Subsequent passages were performed by transferring 10 ml of the enrichment into 90 ml of FeOOH suspended in media. All enrichments were set up in duplicate. All 14 enrichments demonstrated Fe (III) reduction. In general, the cultures reduced about half of the 50 mM Fe(III) floc available. All enrichments maintained Fe(III) reduction through the dilutions.

DNA extraction and characterization by TRFLP

DNA was extracted from up to 5 passages of the enrichment cultures. The presence of 50mM FeOOH in the enrichments interfered with extraction of DNA following standard protocols. Therefore, a new protocol was developed. Using this protocol, total genomic DNA was extracted from the cells, purified and PCR amplified using a fluorescent-labeled primer. Various restriction enzymes were used to cut the DNA. The fluorescent moiety on the end of the digested PCR product was detected using the PE/ABI GeneScan Software, which displays the various terminal restriction fragment length polymorphisms (TRFLP's) as a series of peaks separated on the x-axis by fragment length in number of base pairs. The resulting "fingerprint" of a particular soil/sediment sample had multiple peaks, each corresponding to a different organism.

Similarity values between fingerprints were calculated using Sorenson's index and clustering was performed by the UPGMA (unweighted pair group mean average) method. Sorenson's index is calculated as follows: $S_{ab} = 2 * (N_{ab}/(N_a+N_b))$, where N_a is the number of peaks in fingerprint A, N_b is the number of peaks in fingerprint B, and N_{ab} is the number of shared peaks between the two fingerprints. Presence or absence of the TRFLP peaks allows for 2 samples to be compared using Sorenson's Index: $C_s = 2N_{ab}/(N_a + N_b)$, where N_{ab} is the number of shared peaks between two samples, and N_a and N_b are the number of peaks for samples A and B respectively (13,14). All indices and clusters were calculated using the COMbinatorial Polythetic Agglomerative Hierarchical clustering package (COMPAH96; http://www.es.umb.edu/edgwebp.htm).

A phenogram of the output of this analysis was generated using an unweighted pair group mean average (UPGMA) algorithm (Fig. 1). The cluster diagram shows that the initial enrichments from the various sites formed distinct clusters. The similarity (C_s) value between the Par Pond and LTR 1st dilutions was 0.21, whereas the C_s values within the Par Pond cluster

ranged from 0.40 to 0.85 and those within the LTR cluster from 0.38 to 0.76. For the 3rd dilution cluster intermixing of the enrichments was seen, as evidenced by the presence of two subgroups with members from both the LTR and Par Pond enrichments. C_s values for these subgroups were 0.62 between P3b-3 and S1b-3, and 0.68 between S1a-3 and the P2b-3/P3a-3 group. By the 4th dilution, the enrichment communities were similar enough that the cluster was intermixed with several 3rd dilution enrichments without regard to the origin of the initial sediment/soil inoculum.

Pure culture isolation

Isolates were obtained by spread plating 100 µl from one Par Pond enrichment (P4b-5) and one LTR enrichment (S1b-5) onto agar minimal media plates, containing Fe(III) citrate as the electron acceptor. Plates were incubated anaerobically at room temperature in a Coy chamber and individual colonies were transferred anerobically into 10 ml serum bottles. Seven Fe(III) reducing isolates were obtained from the SRS enrichment cultures, 5 from the Par Pond enrichment P4b-5 and 2 from the LTR enrichment S1b-5. Table 1 lists putative identification of these isolates based on percent similarity of 16S rRNA sequence data to sequences deposited in GenBank. ~1500 bp of double stranded sequence was obtained for each of the isolates. All isolates were able to reduce Fe(III) floc within several days (Table 1). Purity of the isolates was determined by microscopic investigation as well as by plating onto minimal and rich media plates. Uniform colony morphology was obtained for all plates (data not shown). Microscopic investigation initally showed that the PAR2 sample contained two distinct microbes. Replating and picking of individual colonies resulted in obtaining 2 identical *Aeromonas* species. Based on 16S rRNA sequence similarity, isolates from the *Clostridia*, *Bacillus* and *Aeromonas* genera were obtained (Table 1).

II. Measurement of Fe(III) bioavailability

In batch systems, it has been demonstrated that even the most available oxide—amorphous hydrous ferric oxide—cannot be totally consumed in support of microbial respiration *(1,2)*. The inability of microorganisms in batch systems to reduce Fe(III) oxides completely has been attributed to sorption of $Fe(II)_{(aq)}$ to Fe(III) oxide surfaces *(2-6)*, and to formation of magnetite (Fe_3O_4), which consumes 2 moles of Fe(III) for every mole of Fe(II) coprecipitated and renders the Fe(III) unavailable at pH 7 *(7)*. Crystalline Fe(III) oxides are only slightly reducible by DIRB in batch systems *(2,8)*. Thus, 'bioavailable' Fe(III) is often assumed to be only the non-crystalline fraction of the total Fe(III) oxides. Bioavailability then is quantified by extracting the sample with hydroxylamine-HCl solution, which reduces amorphous Fe(III) to soluble Fe(II) but reduces <1% of crystalline Fe(III) oxides *(9)*. Other extraction methods (e.g. acid ammonium oxalate solution) extract amorphous Fe(III) but also extract crystalline Fe(III) from minerals that are not biologically reducible (e.g., magnetite, iron in organic complexes) *(9,10)*. In addition, small amounts of Fe(II) in solution during the acid ammonium oxalate extraction can catalyze the dissolution of magnetite *(11)*, goethite and hematite *(12,13)*, overestimating available Fe(III). Another disadvantage of both hydroxylamine reduction and oxalate extraction is that they are performed under acidic conditions. Acidic conditions inherently mask the biogeochemical processes of $Fe(II)_{(aq)}$ sorption and magnetite precipitation.

In soils, the sequestration of Fe(III) in micropores that bacteria cannot enter is difficult to measure using any soluble chemical treatment since all of these chemicals can diffuse into and

react in micropores. However, many soils contain soluble organic matter that is capable of complexing Fe(III) or of acting as electron shuttles *(14,15)*. In this case, Fe(III) located in micropores is potentially available to bacteria. Thus, it is difficult to predict Fe(III) bioavailability in natural soil systems and the bioavailability of Fe(III) in micropores is not well documented.

The ideal surrogate chemical measurement of bioavailability would be conducted under reaction conditions representative of the microbial electron transfer event. Indirect coulometric titration (ICT) has been used frequently to study electroactive biological systems in which biocomponents exhibit irreversible electrochemical or redox behavior *(16-18)*. In the ICT method, the redox titrant is generated in the reduced state and added to a solution containing the biocomponent to which it transfers electrons. Proper selection of the titrant allows monitoring of the electron transfer via spectrographic changes *(17)*.

The quinol (AHDS) form of 9,10-anthraquinone-2,6-disulfonate (AQDS) was used as a titrant to determine bioavailability of Fe(III) in pure iron minerals and several soils. AHDS oxidation to AQDS was coupled to Fe(III) reduction to Fe(II) in biological media consisting of trace salts and vitamins, providing estimates of bioavailability consistent with the biogeochemical mechanisms and conditions that control Fe(III) availability to iron-reducing bacteria. For comparison of AHDS titration to existing techniques, all samples were treated separately with acid hydroxylamine reduction, acid ammonium oxalate extraction and biological reduction by a model DIRB, *S. alga* BrY. To test for the effects of Fe(III) sequestration in microporous soils, we also treated all soil samples to biological reduction by *S. alga* BrY in batch microcosms containing the oxidized quinone, 9,10-anthraquinone-2,6-disulfonate (AQDS), as a media amendment. In this case AQDS served as an electron shuttle rather than a redox titrant. To quantify the effects of Fe(III) occlusion by sorption of Fe(II), the most reactive synthetic oxide, ferrihydrite, was 'poisoned' with presorbed Fe(II) and then titrated with AHDS. Because our measurements were made in biological media under typical growth conditions and soil pH, Fe(III) reduced by AHDS could adsorb or precipitate (as magnetite, siderite ($FeCO_3$) or vivianite ($Fe_3(PO_4)_2 \cdot 8H_2O$)) as it would under microbial Fe(III)-reducing conditions.

For ferrihydrite (SA = 230 $m^2\ g^{-1}$), AHDS titration, hydroxylamine-HCl reduction, and oxalate extraction all measured 100% of the total Fe present. Biological activity was much lower than chemical activity, with only 6% of the total Fe reduced (Figure 2). Approximately 60% of the HSA goethite (SA = 140 $m^2\ g^{-1}$) was available to oxalate extraction, which is greater than other reported values for this mineral *(2)*. Hydroxylamine-HCl reduced about one third of the biologically available Fe(III); AHDS titration was intermediate between oxalate extraction and hydroxylamine-HCl reduction, producing about 1.5 times more Fe(II) than observed through biological reduction (Figure 2). The two low surface area oxides, LSA goethite (22 $m^2\ g^{-1}$) and hematite (11 $m^2\ g^{-1}$), exhibited similar behavior (Figure 2, inset). LSA goethite, with double the surface area of hematite, had almost twice as much biologically reducible Fe(III) per unit mass. However, LSA goethite was 15% less available to oxalate extraction than was hematite (Figure 1, inset). Very little Fe(III) in these oxides was reduced by hydroxylamine-HCl (0.29% of total Fe for LSA goethite and 0.75% of total Fe for hematite).

In both size fractions of the Donora Station and Tabernacle Church soil, biological reduction was statistically the same as hydroxylamine-HCl reducible or oxalate extractable Fe(III) measurements; however, AHDS titration exceeded these measurements by more than two-fold in some cases (Figure 3). Stinson's Bridge soil has anomalous results for oxalate

extraction, which would normally extract all the amorphous Fe(III) and some of the crystalline Fe(III) oxides. However, oxalate extracted one-third to one quarter of the Fe that was extracted by hydroxylamine-HCl or biologically reduced. Biological reduction of the Stinson's Bridge soil was the same as hydroxylamine-HCl reduction in the smaller size fraction (<500 μm), but in the larger size fraction (500-1000 μm) hydroxylamine-HCl reduction overestimated biological reduction by approximately 40% (Figure 3). Once again, AHDS overestimated biological reduction by over two-fold, and in fact reduced nearly all of the total Fe in the soils (>100% for the smaller size fraction) (Figure 3).

When AQDS was added to the biological media at the start of the experiment to act as an electron shuttle, the amount of bioavailable Fe(III) on a mass basis increased dramatically for most soils. For the Donora Station soil and Tabernacle Church soil the biological reduction with AQDS was similar to the estimated bioavailability calculated by AHDS titration. For the Stinson's Bridge soil, the bioavailable Fe(III) was still overestimated by AHDS titration even though biological reduction almost doubled with this amendment. Biological reduction with AQDS also was more rapid than without AQDS, reaching the endpoint within 10 days instead of 44 days of incubation.

Our results indicate that much of the Fe(III) in these soils is present in micropores, preventing direct contact of bacteria with this fraction of the Fe(III). The agreement of hydroxylamine-HCl reduction with biological reduction in the absence of AQDS suggests that the amorphous Fe(III) is located on the exterior of particles where it is accessible to direct contact with DIRB. The addition of an electron shuttle increases the Fe(III) bioavailability by transporting electrons in the aqueous phase to Fe(III) oxides inaccessible to bacteria. The failure of hydroxylamine-HCl reduction and oxalate extraction to predict this degree of Fe(III) bioavailability suggests that the predominant Fe(III) oxide forms within the micropores of these soils are crystalline Fe(III) oxides. This finding also supports our hypothesis that AHDS titration of Fe(III) oxides is mechanistic and more representative of a biological system than the other chemical reduction/extraction techniques. Soil microporosity is shown to create a significant limitation to the extent of Fe(III) reduction in natural systems without electron shuttles

III. Kinetics modeling

Model overview

In the kinetics model, $Fe^{3+}_{(aq)}$, Fe^{3+} oxides or soluble electron shuttles are all potential electron acceptors for bacterial respiration. The sole carbon and energy source is the electron donor lactate ($CH_3CHOHCOO^-$). Lactate is incompletely reduced to acetate (CH_3COO^-) and carbon dioxide (CO_2), with some of the carbon diverted to biomass ($C_5H_7O_2N$). Carbon dioxide is in equilibrium with bicarbonate (HCO_3^-) and is referenced as such. The stoichiometry of Fe^{3+} reduction and biomass formation (on an electron mole basis) is given by:

$$\begin{aligned} &Fe(III) + 0.25(1+Y_{b/EA})\,CH_3CHOHCOO^- + (0.05Y_{b/EA})\,NH_3 + (0.5-0.15Y_{b/EA})\,H_2O = \\ &Fe(II) + 0.25\,HCO_3^- + 0.25(1+Y_{b/EA})\,CH_3COO^- + 1.25\,H^+ + (0.05Y_{b/EA})\,C_5H_7O_2N \end{aligned} \quad (1)$$

Electron shuttles can be represented by a similar equation but they generally have the potential to accept twice as many electrons as Fe^{3+} and they require different yield coefficients.

Iron(III) reduction generates $Fe^{2+}_{(aq)}$ through reductive dissolution. Iron(II)$_{(aq)}$ then partitions into the solid phase via sorption and siderite ($FeCO_3$) precipitation. Sorbed Fe^{2+} is assumed to coat solid phase Fe^{3+} and remove it from the pool of bioavailable Fe^{3+} in the ratio of 2 Fe^{3+}: 1 Fe^{2+}, the ratio found in magnetite. Siderite precipitation occurs only when the solution is supersaturated with respect to ferrous iron and carbonate.

Bacterial reduction of electron shuttles produces soluble chemical species capable of reducing Fe^{3+} abiotically. The $Fe^{2+}_{(aq)}$ resulting from this redox transformation is subject to the same reactions as Fe^{2+} produced biogenically.

In all, this model computes the fate of four solid components and five dissolved components. Numbered consecutively for reference within the model (per Table 2), the four solids are: (1) biomass, (2) solid Fe^{3+} in the form of Fe^{3+} oxides, (3) solid Fe^{2+} in the form of adsorbed Fe^{2+}, and (4) solid Fe^{2+} in the form of precipitated Fe^{2+} minerals. The six aqueous components are: (5) dissolved Fe^{3+} as either a free ion or a chelated/complexed species, (6) dissolved Fe^{2+} as a free ion or a chelated/complexed species, (7) oxidized and (8) reduced electron shuttles, and (9) dissolved CO_2 as bicarbonate.

Kinetics of electron acceptor reduction

Biological reduction of electron acceptors follows typical Monod kinetics. In this model we consider only the electron acceptor utilization to be rate limiting, such that there is no need for Monod representation of organic carbon. In other words, at all times substrate is present in sufficient excess that reduction is zero order with respect to substrate. We have done this so that we can experimentally elucidate the kinetics associated only with Fe^{3+} bioavailability and reduction. The model incorporates microbial reduction kinetics from three potential electron acceptors: solid Fe^{3+} oxide, chelated Fe^{3+} and any other electron accepting species that can act as an electron shuttle. The electron shuttle must satisfy two criteria: (i) it must be soluble and (ii) it must have a reduction potential between that of the Fe^{3+}/Fe^{2+} couple and the substrate/CO_2 couple. All three of the electron acceptors behave according to Monod-type kinetics; however, systems containing more than one electron acceptor will be affected by interactions between the acceptors. The two interactions considered are (i) the inhibition of utilization of one electron acceptor by another due to competition for the active enzymatic site and (ii) fortuitous electron acceptor utilization from the presence of multiple substrates. Electron acceptor utilization is due to all species present *(19-21)*:

$$\mu_T = \sum_{i=1}^{n} \mu_i \tag{2}$$

where n is the number of substrates and μ_i is the specific utilization rate of electron acceptor i:

$$\mu_i = \hat{\mu}_i \left(\frac{C_i}{K_{Si} + \sum_{j=1}^{n} \frac{K_{Si}}{K_{Sj}} C_j} \right) \tag{3}$$

The concentration of all soluble electron acceptors is the molar solution concentration. The concentration of the solid Fe^{3+} oxides depends in a complicated way on surface area and bacterial coverage of this surface. Therefore, we have normalized "bioavailable Fe^{3+}" to surface area and surface coverage by bacteria, such that the concentration of solid Fe^{3+} used in Eq. (3) is:

$$C_{Fe(III),solid} = \frac{X_b}{W_{Fe^{3+}}} \tag{4}$$

where $W_{Fe^{3+}}$ is a measure of the total number of surface sites of reactive Fe^{3+}. From Fe^{3+} oxide concentration in units of total Fe^{3+}, $W_{Fe^{3+}}$ can be calculated from the oxide surface area, unit cell weight, and surface site density. This conversion is dependent therefore on the type of oxide present. We find that normalization such as in (4) can be supported by data published by *(2)* (1996; Figure 3, *ref. cit.*), for which the following expression describes their data:

$$\frac{1}{W_{Fe^{3+}}}\frac{dX_{Fe^{3+}}}{dt} = \hat{\eta}\left(\frac{\frac{X_b}{W_{Fe^{3+}}}}{K_\eta + \frac{X_b}{W_{Fe^{3+}}}}\right) \tag{5}$$

The approach of measuring Monod parameters in single electron acceptor systems and applying them to the multiple electron acceptor system is valid assuming that the microbial community is in the same physiological state in the mixed system as it is in the single electron acceptor system and that the electron acceptors all use a common enzyme system *(22)*.

Mineral precipitation/dissolution reactions

The major Fe^{2+} mineral species found in Fe^{3+} reducing systems are siderite and magnetite *(23,24)*. Magnetite precipitation is accounted for empirically in this model, as discussed later. Based on our experimental design *(25)* we found that there was little possibility for the supersaturation and precipitation of vivianite ($Fe_3(PO_4)_2 \cdot 8H_2O$) at the low phosphate levels used in our media (c.a. 0.5 mM total PO_4).

It has been hypothesized that siderite precipitation does not occlude any solid Fe^{3+} sites, but instead acts as an Fe^{2+} sink *(26)*. We have also considered the case in which siderite precipitates on and partially occludes active Fe^{3+} reduction sites. Siderite precipitation is relatively slow and is unlikely to have a major effect on experiments with short durations, but is very likely to affect results in natural systems or in experiments with longer time frames.

Electron shuttle interactions

Based on our preliminary experimental evidence (data not shown), reduction of solid Fe^{3+} by electron shuttles is assumed to be first order in electron shuttle concentration and first order in available solid Fe^{3+} surface sites. To complete the electron shuttle cycle, the model includes a Monod-type rate of biotic electron shuttle reduction.

Equilibrium reactions

For low-surface area goethite and amorphous Fe^{3+} oxyhydroxide the rate of sorption is nearly instantaneous on the time-scale of interest for our model *(25)*, so Fe^{2+} sorption and the concurrent loss of bioavailable Fe^{3+} is treated at each time step as an equilibrium reaction. The sorption data indicates a Freundlich type isotherm *(6,25)* described by:

$$\frac{X_{Fe^{2+},s}}{W_{Fe^{3+}}} = K_f S_{Fe^{2+}}{}^{N_f} \tag{6}$$

Loss of bioavailable Fe^{3+} due to Fe^{2+} sorption is assumed to follow magnetite stoichiometry of one mole of Fe^{3+} lost for every two moles of Fe^{2+} sorbed. Iron(II) sorption is assumed to occur uniformly on all surfaces and precipitation of siderite does not directly impact available Fe^{3+} (e.g. by precipitating on Fe^{3+} surfaces). The precipitation of magnetite is implicitly incorporated into the model via the empirical coefficient relating the Fe^{2+} sorption to loss of bioavailable solid Fe^{3+}.

Modeling strategy

The full kinetic model contains four solid components and five aqueous components, participating in seven kinetically controlled processes and one equilibrium exchange. These components and the kinetic process rates are listed in Table 1. This table was developed assuming lactate as the sole carbon source, ammonia as the source of biomass nitrogen, and a biomass chemical composition of $C_5H_7O_2N$. The table is written on an electron molar basis and assumes that 1 mole of electron shuttle is capable of accepting 2 electrons. Differential equations can be derived from this table by multiplying each component cell by the associated process rate in the right-hand column and summing the components within a column. Note that siderite precipitation and dissolution cannot occur simultaneously. As an example, of all nine species considered dissolved Fe^{2+} is involved in the most processes and has the most complex differential equation. The differential equation describing the kinetics of dissolved Fe^{2+} formation in a supersaturated ferrous carbonate solution is derived by multiplying the coefficients for processes *a, b, d,* and *e* by the appropriate process rate in the right-hand column and adding the terms:

$$\frac{\partial S_{Fe^{2+}}}{\partial t} = W_{Fe^{3+}}\hat{\eta}\left(\frac{\frac{X_b}{W_{Fe^{3+}}}}{K_{S(\eta)} + \frac{K_{S(\eta)}}{K_{S(Fe^{3+})}}S_{Fe^{3+}} + \frac{K_{S(\eta)}}{K_{S(Es+)}}S_{Es+} + \frac{X_b}{W_{Fe^{3+}}}}\right)$$
$$+\frac{20X_b}{Y_{b/SFe}}\hat{\mu}_{Fe^{3+}}\left(\frac{S_{Fe^{3+}}}{K_{S(Fe^{3+})} + \frac{K_{S(Fe^{3+})}}{K_{S(\eta)}}\frac{X_b}{W_{Fe^{3+}}} + \frac{K_{S(Fe^{3+})}}{K_{S(Es+)}}S_{Es+} + S_{Fe^{3+}}}\right) + 2k_1 W_{Fe^{3+}} S_{ES-} - k_2(\Omega - 1) \tag{7}$$

The nine differential equations along with the time-independent sorption equation were solved using an ODE solver package (STELLA 7.0, High Performance Systems, Inc.), using Euler's method. Initial concentrations were set according to common concentrations used in our experiments or found in the literature (Table 3). Baseline parameter values were varied over several orders of magnitude centered on initial estimates (Table 4). Selection of these parameter values was based on data in the current literature or data collected in our own independent laboratory experiments.

This model was used to simulate microbial Fe(III) reduction under a number of conditions of interest. For instance, the model was used to compare two different formulations for the precipitation of siderite, which acts as a major mineralogical control to the extent of Fe(III) oxide reduction. Van Cappellan and Wang (VW) have used a formulation based on a linear rate law with respect to the degree of supersaturation of Fe^{2+} and CO_3^{2-} in the aqueous phase *(27)*. Alternatively, Wajon, Ho and Murphy (WHM) have used a formulation depending on a linear rate law with respect to the square of relative aqueous phase supersaturation *(28)*. The WHM model was determined empirically from samples containing ferrous carbonate minerals (aragonite). The precipitation rates found in this model were greater than those observed in systems containing no natural aragonite. Thus, the VW model is considered to be more general.

In the first case we assumed that siderite acted only as a sink for aqueous Fe^{2+}, thereby limiting the sorption of Fe^{2+} onto Fe^{3+} oxides. In this case, the Fe^{3+} reduction rate and final Fe^{3+} oxide concentration were unaffected by siderite precipitation (Figure 4A). However, there was far less dissolved Fe^{2+} under the WHM model than the VW model (Figure 4B). In all three models the Fe^{3+} oxide surfaces became saturated with sorbed Fe^{2+} to essentially the same concentration (data not shown). Therefore, any additional Fe^{2+} phase, such as siderite, was formed at the expense of dissolved Fe^{2+}. Siderite precipitated more rapidly according to the WHM model than the VW model (Figure 4C), and resulted in a higher final siderite concentration.

In the second case, siderite precipitation was assumed to occur on the Fe^{3+} oxide surface, depleting the bioavailable Fe^{3+} in a 1:1 stoichiometry. The initial Fe^{3+} reduction rate wais the same for all three cases, but the extent of reduction decreased as a function of siderite precipitation (Figure 5A). The WHM model caused Fe^{3+} reduction to cease after about 50% of the total Fe^{3+} is reduced, compared to 75% reduction for the VW model and over 85% for the model that did not allow siderite precipitation. Siderite precipitation had a similar effect on dissolved Fe^{2+} concentration in this case (Figure 5B) as it did in the first case (i.e., the WHM model maintained very low solution Fe^{2+} concentrations). The mass of siderite formed in this case was less than in the previous case because Fe^{3+} reduction is shut down early due to site occlusion (Figure 5C).

Nomenclature

X_b biomass concentration, [mole biomass L^{-1}]

$X_{Fe^{3+}}$ solid-phase Fe^{3+} concentration, [mole Fe^{3+} L^{-1}]

$X_{Fe^{2+},s}$ sorbed Fe^{2+} concentration, [mole $Fe^{2+}_{(s)}$ L^{-1}]

$X_{Fe^{2+},p}$ siderite concentration, [mole $Fe^{2+}_{(s)}$ L^{-1}]

$S_{Fe^{3+}}$ dissolved Fe^{3+} concentration, [mole $Fe^{3+}_{(aq)}$ L^{-1}]

$S_{Fe^{2+}}$ dissolved Fe^{2+} concentration, [mole $Fe^{2+}_{(aq)}$ L^{-1}]

S_{Es+} oxidized electron shuttle concentration, [mole e^- equivalent L^{-1}]

S_{Es-} reduced electron shuttle concentration, [mole e^- equivalent L^{-1}]

$S_{HCO_3^-}$ dissolved carbonate concentration, [mole C L^{-1}]

$W_{Fe^{2+}}$ solid-phase Fe^{3+} surface site density, [mole surface Fe^{3+} sites L^{-1}]

$Y_{b/XFe}$ solid Fe^{3+} yield coefficient, [mole e^- to biomass / moles e^- to $Fe^{3+}_{(s)}$]

$Y_{b/SFe}$ chelated Fe^{3+} yield coefficient, [mole e^- to biomass / moles e^- to $Fe^{3+}_{(aq)}$]

$Y_{b/Es}$ electron shuttle yield coefficient, [mole e^- to biomass / moles e^- to shuttle]

$\hat{\eta}$ max. biological Fe^{3+} reduction rate (solid), [mole Fe^{3+} (mole surface Fe^{3+})$^{-1}$ hr^{-1}]

$\hat{\mu}_{Fe^{3+}}$ maximum biological Fe^{3+} reduction rate (aqueous), [hr^{-1}]

$\hat{\mu}_{Es+}$ maximum biological e^- shuttle reduction rate, [hr^{-1}]

$K_{S(\eta)}$ Fe^{3+} oxide surface half-saturation constant, [mole biomass / mole surface Fe^{3+}]

$K_{S(Fe^{3+})}$ Fe^{3+} half-saturation constant, [mole $Fe^{3+}_{(aq)}$ L^{-1}]

$K_{S(Es+)}$ electron shuttle half-saturation constant, [mole e^- equivalent L^{-1}]

k_1 Fe^{2+} adsorption rate constant, [mole e^- to surface Fe^{3+} / (mole e^- from shuttle · mole surface Fe^{3+} · hr)$^{-1}$]

k_2 siderite precipitation rate constant, [mole $Fe^{2+}_{(s)}$ L^{-1} hr^{-1}]

k_{-2} siderite dissolution rate constant, [hr^{-1}]

K_2 siderite equilibrium constant, [(mole $Fe^{2+}_{(aq)}$ L^{-1}) (mole HCO_3^- L^{-1})]

b bacterial decay rate, [hr^{-1}]

K_f Freundlich isotherm coefficient

N_f Freundlich isotherm coefficient

μ_T overall multi-component reduction rate [hr^{-1}]

μ_i individual component reduction rate [hr^{-1}]

$\hat{\mu}_i$ individual component maximum reduction rate [hr^{-1}]

C_i, C_j individual component concentration [mole L^{-1}]

K_{Si}, K_{Sj} individual component half-saturation coefficient [mole L^{-1}]

$C_{Fe(III),solid}$ biomass coverage of Fe(III) surface [mole biomass / mole Fe(III) surface sites]

$$Eq1 \equiv W_{Fe^{3+}} \hat{\eta} \left(\frac{\frac{X_b}{W_{Fe^{3+}}}}{K_{S(\eta)} + \frac{K_{S(\eta)}}{K_{S(Fe^{3+})}} S_{Fe^{3+}} + \frac{K_{S(\eta)}}{K_{S(Es+)}} S_{Es+} + \frac{X_b}{W_{Fe^{3+}}}} \right)$$

$$Eq2 \equiv \frac{20 X_b}{Y_{b/SFe}} \hat{\mu}_{Fe^{3+}} \left(\frac{S_{Fe^{3+}}}{K_{S(Fe^{3+})} + \frac{K_{S(Fe^{3+})}}{K_{S(\eta)}} \frac{X_b}{W_{Fe^{3+}}} + \frac{K_{S(Fe^{3+})}}{K_{S(Es+)}} S_{Es+} + S_{Fe^{3+}}} \right)$$

$$Eq3 \equiv \frac{20 X_b}{Y_{b/Es}} \hat{\mu}_{Es+} \left(\frac{S_{Es+}}{K_{S(Es+)} + \frac{K_{S(Es+)}}{K_{S(\eta)}} \frac{X_b}{W_{Fe^{3+}}} + \frac{K_{S(Es+)}}{K_{S(Fe^{3+})}} S_{Fe^{3+}} + S_{Es+}} \right)$$

$$\Omega = \frac{S_{Fe^{2+}} S_{HCO_3^-}}{K_2}$$

References

(1) Lovley, D. R.; Phillips, E. J. P. *Appl. Environ. Microbiol.* **1986**, *52*, 751-757.

(2) Roden, E. E.; Zachara, J. M. *Environ. Sci. Technol.* **1996**, *30*, 1618-1628.

(3) Kostka, J. E.; Haefele, E.; Viehweger, R.; Stucki, J. W. *Environ. Sci. Technol.* **1999**, *33*, 3127-3133.

(4) Roden, E. E.; Urrutia, M. M. *Environ. Sci. Technol.* **1999**, *33*, 1847-1853.

(5) Urrutia, M. M.; Roden, E. E.; Fredrickson, J. K.; Zachara, J. M. *Geomicrobiol.* **1998**, *15*, 269-291.

(6) Urrutia, M. M.; Roden, E. E.; Zachara, J. M. *Environ. Sci. Technol.* **1999**, *33*, 4022-4028.

(7) Kostka, J. E.; Nealson, K. H. *Environ. Sci. Technol.* **1995**, *29*, 2535-2540.

(8) Lovley, D. R.; Phillips, E. J. P. *Appl. Environ. Microbiol.* **1988**, *54*, 1472-1480.

(9) Chao, T. T.; Zhou, L. *Soil Sci. Soc. Amer. J.* **1983**, *47*, 225-232.

(10) Schwertmann, U. *Can. J. Soil Sci.* **1973**, *53*, 244-246.

(11) Blesa, M. A.; Marinovich, H. A.; Baumgartner, E. C.; Maroto, A. J. G. *Inorg. Chem.* **1987**, *26*, 3713-3717.

(12) Suter, D.; Siffert, C.; Sulzberger, B.; Stumm, W. *Naturwiss* **1988**, *75*, 571-573.

(13) LaKind, J. S.; Stone, A. T. *Geochim. Cosmochim. Acta* **1989**, *53*, 961-972.

(14) Gamble, D. S.; Schnitzer, M. In *Trace Metals and Metal-Organic Interactions in Natural Waters*; Singer, P. C., Ed.; Ann Arbor Science Publishers: Ann Arbor, MI, 1973; pp 265-302.

(15) Lovley, D. R.; Blunt-Harris, E. L. *Appl. Environ. Microbiol.* **1999**, *65*, 4252-4254.

(16) Clark, W. M. *Oxidation-Reduction Potentials of Organic Systems*; The Williams & Wilkins Company: Baltimore, MD, 1960.

(17) Szentrimay, R.; Yeh, P.; Kuwana, T. In *Electrochemical Studies of Biological Systems.*; Sawyer, D. T., Ed.; American Chemical Society: Washington, D.C., 1977; Vol. 38, pp 143-169.

(18) Fultz, M. L.; Durst, R. A. *Anal. Chem. Acta* **1982**, *140*, 1-18.

(19) Autho; State University of New York at Buffalo: Buffalo, NY, 1994.

(20) Guha, S.; Peters, C. A.; Jaffe, P. R. *Biotech. Bioeng.* **1999**, *65*, 491-499.

(21) Smouse, P. *Theoret. Pop. Biol.* **1980**, *17*, 16-36.

(22) Guha, S.; Jaffe, P. R. *Biotech. Bioeng.* **1996**, *50*, 693-699.

(23) Bell, P. E.; Mills, A. L.; Herman, J. S. *Appl. Environ. Microbiol.* **1987**, *53*, 2610-2616.

(24) Roden, E. E.; Lovley, D. R. *Appl. Environ. Microbiol.* **1993**, *59*, 734-742.

(25) Hacherl, E. L.; Kosson, D. S.; Young, L. Y.; Cowan, R. M. *Unpublished data.* **2001**.

(26) Fredrickson, J. K.; Zachara, J. M.; Kennedy, D. W.; Dong, H.; Onstott, T. C.; Hinman, N. W.; Li, S.-M. *Geochim. Cosmochim. Acta* **1998**, *62*, 3239-3257.

(27) van Cappellen, P.; Wang, Y. In *Metal Contaminated Aquatic Sediments*; Allen, H. E., Ed.; Ann Arbor Press: Chelsea, MI, 1995.

(28) Wajon, J. E.; Ho, G.-E.; Murphy, P. J. *Wat. Res.* **1985**, *19*, 831-837.

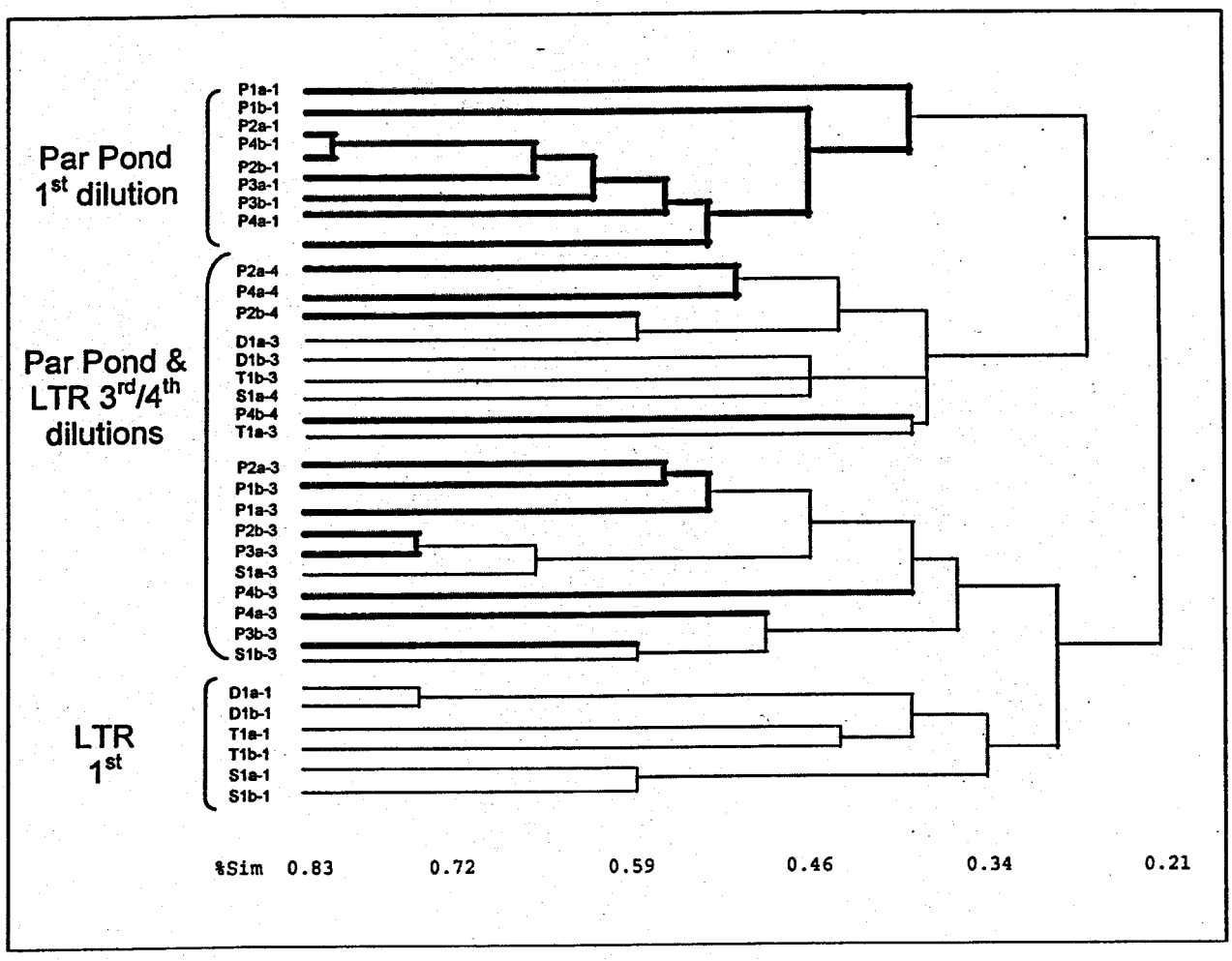

Figure 1 – Cluster diagram of similarity values for T-RFLP samples. Similarity levels are indicated below the diagram. In this figure, upper case letters refer to sample site, lower case letters indicate replicates and the dashed number is the passage number. D = Donora Station; P = Par Pond; S = Stinson's Bridge; T = Tabernacle Church. Thickened lines in the figure correspond to Par Pond samples, while thinner lines indicate LTR samples.

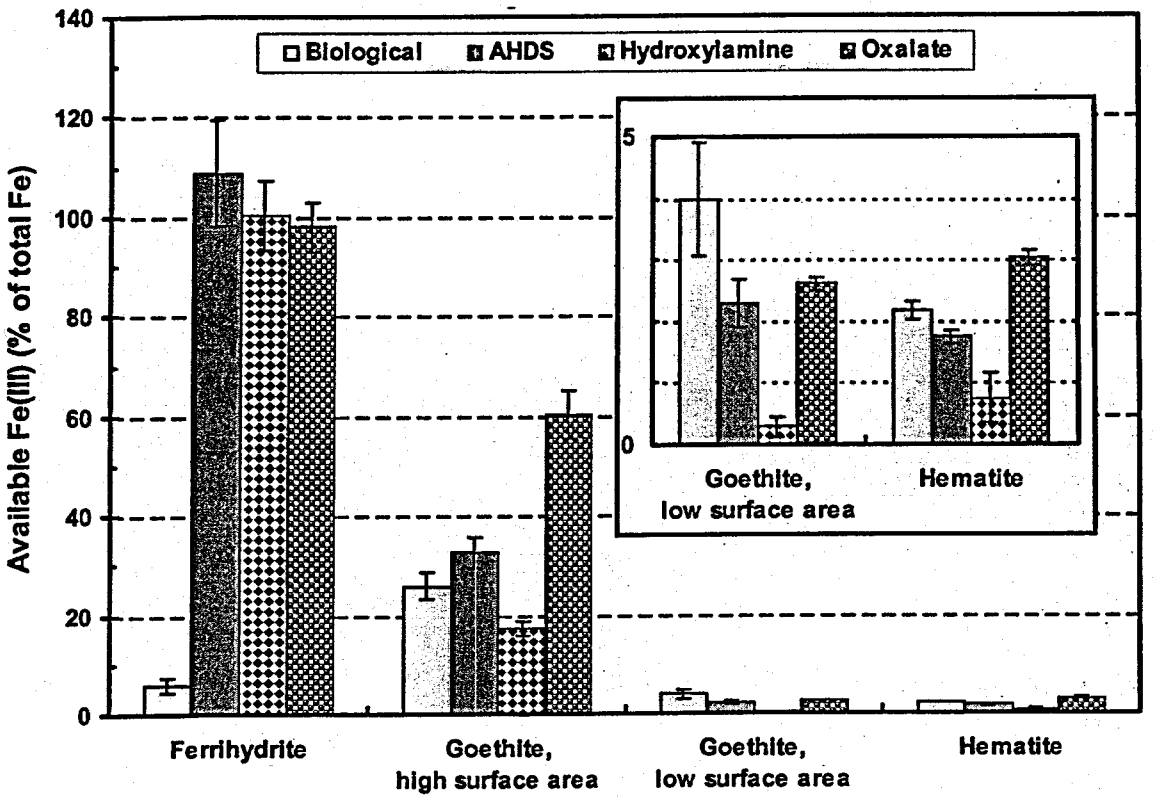

Figure 2 – Extent of Fe(III) reduction or extraction in amorphous and crystalline synthetic oxides as a percent of total initial Fe. Error bars indicate 95% confidence intervals of three replicate measurements for chemical treatments and five replicate measurements of biological reduction.

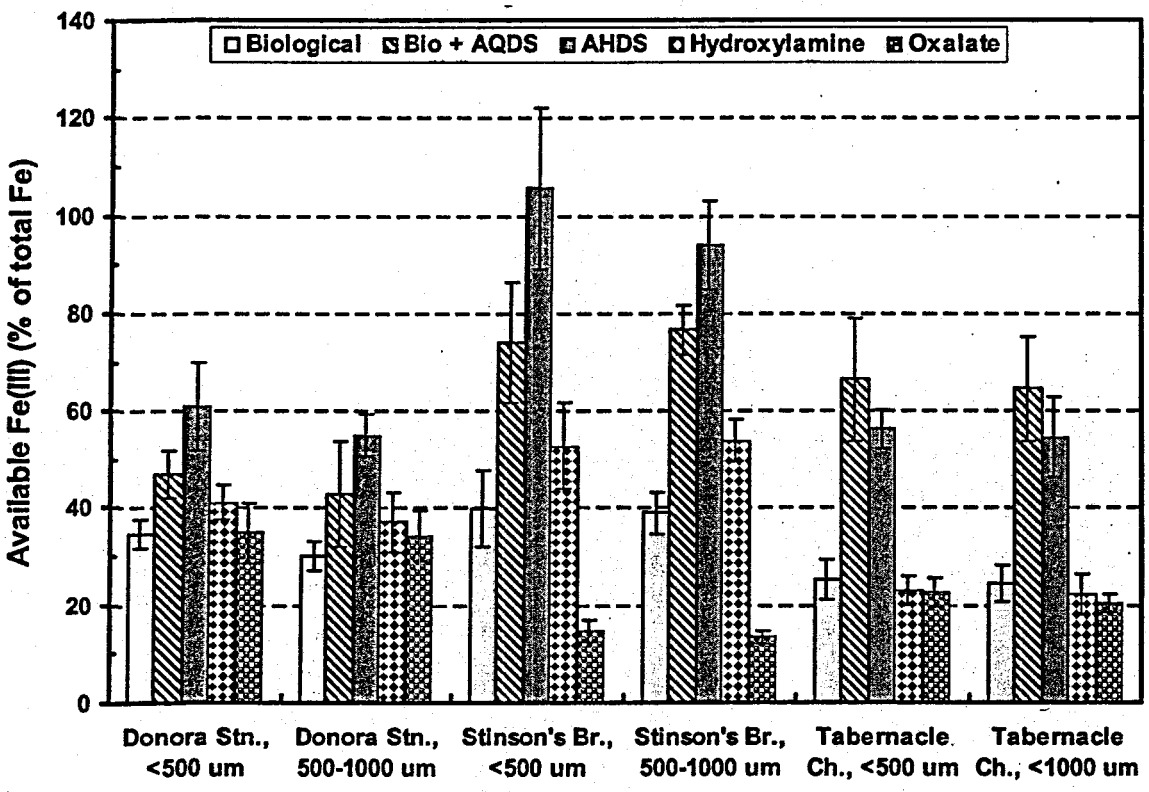

Figure 3 – Extent of Fe(III) reduction or extraction in SRS Site soils as a percent of total initial Fe. Error bars indicate 95% confidence intervals of three replicate measurements for chemical treatments and five replicate measurements of biological reduction.

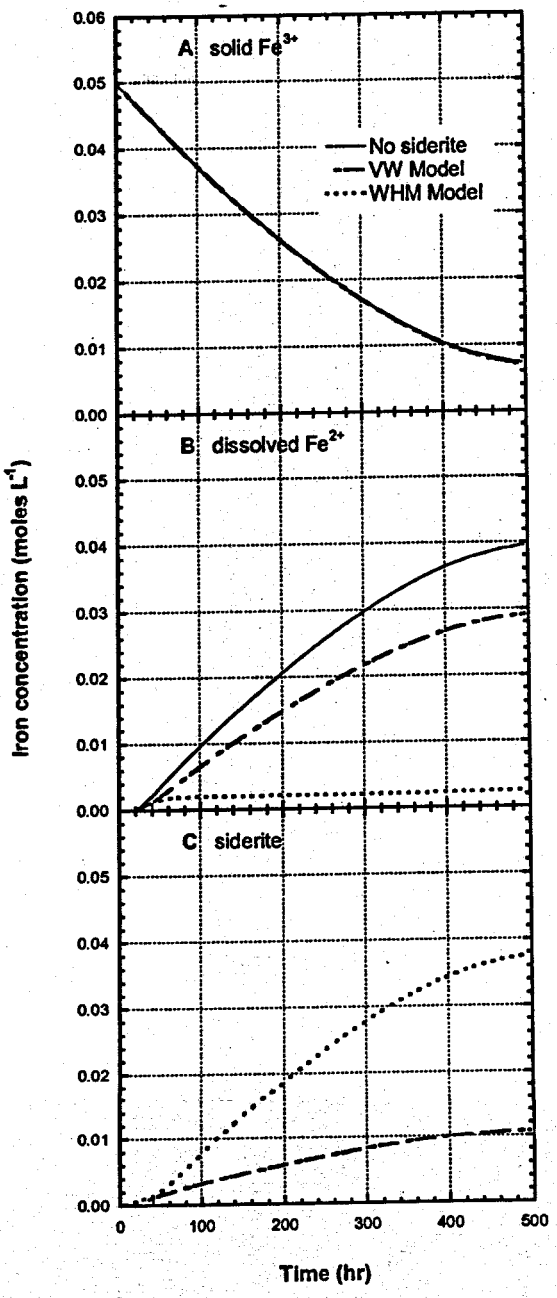

Figure 4 – Comparison of Fe speciation during microbial reduction with concurrent siderite precipitation. Siderite precipitation is modeled using VW and WHM formulations and compared to the case of no siderite precipitation. There are no further interactions between siderite and Fe^{3+} oxides after precipitation. Iron species are (A) total (available + unavailable) solid Fe^{3+}, (B) dissolved Fe^{2+}, and (C) Fe^{2+} as siderite.

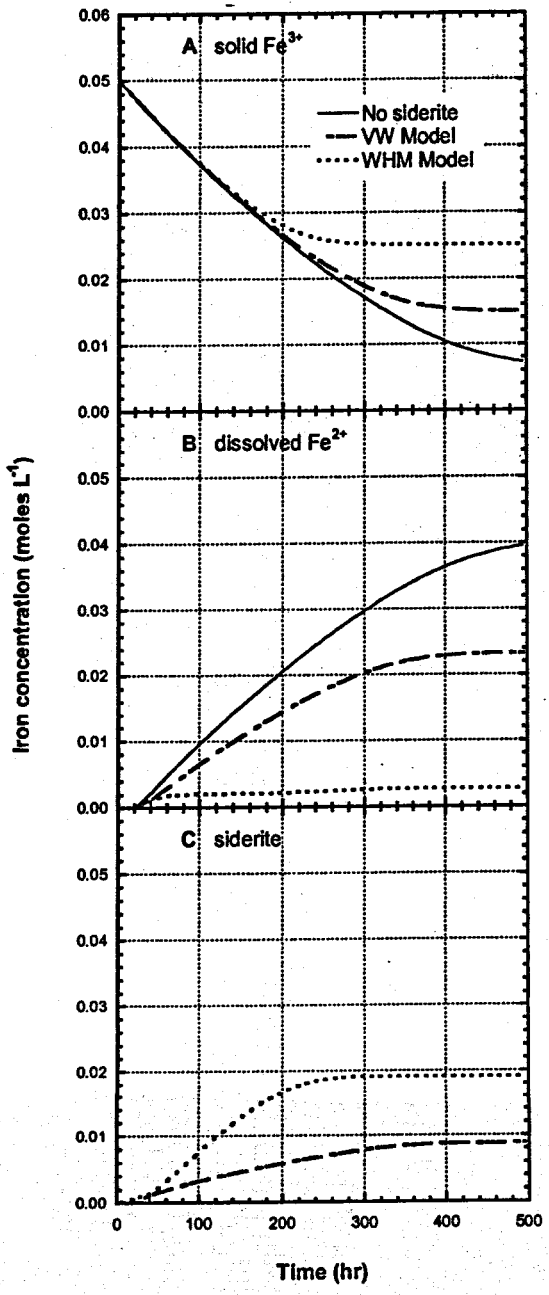

Figure 5 – Comparison of Fe speciation during microbial reduction with concurrent siderite precipitation. Siderite precipitation is modeled using VW and WHM formulations and compared to the case of no siderite precipitation. Siderite precipitation decreased available Fe^{3+} in a 1:1 stoichiometry. Iron species are (A) total (available + unavailable) solid Fe^{3+}, (B) dissolved Fe^{2+}, and (C) Fe^{2+} as siderite.

Table 1 – Isolate data. Names are assigned based on percent similarity of 16S rDNA to known organisms. Isolates were obtained by spread plating from enrichment dilutions onto Fe(III) plates and then transferring colonies into Wolfe's minimal media with 25 mM Fe(III) floc. Isolates were grown on 0.1X TSB and 12.5 mM Fe(III) citrate to obtain iron reduction rate data. Fe(II) production was measured spectrophotometrically using the ferrozine method.

Isolate	16S rDNA (bp sequenced)	Closest relative	Fe(II) produced (mM per day)
Par1	287	*Clostridium estertheticum (96%)*	0.39
Par2	1476	*Aeromonas salmonicida* (97%)	0.55 1st 1.15 2nd
Par3	1476	*Aeromonas salmonicida* (97%)	0.61
Par4	1490	*Bacillus megaterium* (97%)	0.24
Par5	1496	*Bacillus sphaericus* (93%)	0.50
LTR1	na	na	0.50
LTR2	na	na	0.24

Table 2 – Kinetics model for microbial Fe^{3+} reduction. Ordinary differential equations can be derived from this matrix for eight of the nine components considered in the model. Component (4) is sorbed Fe^{2+} and is only involved in equilibrium reactions.

Process	Components								Process rate
	(1) X_b	(2) $X_{Fe^{3+}}$	(3) $X_{Fe^{2+}}$	(5) $S_{Fe^{3+}}$	(6) $S_{Fe^{2+}}$	(7) S_{Es+}	(8) S_{Es-}	(9) $S_{HCO_3^-}$	
(a) Biomass growth on solid Fe	$\frac{1}{20}Y_{b/XFe}$	- 1			+ 1			$\frac{1}{4}$	*Eq*1
(b) Biomass growth on chelated Fe	$\frac{1}{20}Y_{b/SFe}$			- 1	+ 1			$\frac{1}{4}$	*Eq*2
(c) Biomass growth on Electron shuttle	$\frac{1}{20}Y_{b/Es}$					$-\frac{1}{2}$	$\frac{1}{2}$	$\frac{1}{4}$	*Eq*3
(d) Abiotic Fe reduction		- 2			+ 2	+ 1	- 1		$k_1 W_{Fe^{3+}} S_{Es-}$
(e) Fe^{2+} precipitation			+ 1		+ 1			+ 1	$k_2(\Omega - 1) \quad \Omega \geq 1$ (VCW) $k_2\left((K_2\Omega)^{1/2} - K_2^{1/2}\right)^2 \quad \Omega \geq 1$ (WHM).
(f) Fe^{2+} dissolution			+ 1		+ 1			+ 1	$k_{-2} X_{Fe^{2+}} (\Omega - 1) \quad \Omega < 1$
(g) Biomass decay	- 1								bX_b

Table 3 – Initial conditions used in simulations.

Variable	Initial condition
X_b	3.6×10^{-4}
$X_{Fe^{3+}}$	0.050
$X_{Fe^{2+}}$	0
$S_{Fe^{3+}}$	0.050
$S_{Fe^{2+}}$	0
S_{Es+}	0.001
S_{Es-}	0
$S_{HCO_3^-}$	0

Table 4 – Parameter base values and ranges used in kinetics model simulations.

Parameter	Base Value	Range or Individual values
$Y_{b/XFe}$	4.6×10^{-3}	$4.6\times10^{-4} - 4.6\times10^{-2}$
$Y_{b/SFe}$	4.6×10^{-3}	NA
$Y_{b/Es}$	2.3×10^{-3}	NA
$\hat{\eta}$	0.091	0.045 – 0.182
$\hat{\mu}_{Fe^{3+}}$	3.7×10^{-4}	NA
$\hat{\mu}_{Es+}$	2.0×10^{-4}	NA
$K_{S(\eta)}$	0.21	0.11 – 0.42
$K_{S(Fe^{3+})}$	8.2×10^{-3}	NA
$K_{S(Es+)}$	9.2×10^{-4}	NA
k_1	672	0 – 6720
k_2 (WHM)	2.1×10^{5}	NA
k_2 (VW)	5.7×10^{-9}	$5.7\times10^{-10} - 5.7\times10^{-8}$
k_{-2}	5.7×10^{-9}	NA
K_2	$10^{-10.55}$	$10^{-4.4}$, $10^{-8.4}$
b	1×10^{-3}	$1\times10^{-4} - 1\times10^{-2}$
Kf	0.45 (AFO)	2.0†, 12.8††
Nf	0.08 (AFO)	0.16†, 0.43††

† MSA-Gt, †† LSA-Gt